Quantifying mesh textile and effective porosities: A straightforward image analysis procedure for morphological analysis of surgical meshes

Computer Methods and Programs in Biomedicine 242 (2023) 107850

Contents lists available at ScienceDirect

Computer Methods and Programs in Biomedicine

journal homepage: www.elsevier.com/locate/cmpb

# Quantifying mesh textile and effective porosities: A straightforward image analysis procedure for morphological analysis of surgical meshes

Vincenzo Giacalone [a,b,*], Vittoria Civilini [a,b], Alberto L. Audenino [a,b], Mara Terzini [a,b]

[a] Department of Mechanical and Aerospace Engineering, Politecnico di Torino, Turin 10129, Italy
[b] Polito[BIO]Med Lab, Politecnico di Torino, Turin 10129, Italy

ARTICLE INFO

*Keywords:*
Textile porosity
Effective porosity
Surgical mesh
Image analysis

ABSTRACT

*Background and objectives:* Surgical meshes have demonstrated greater reliability compared to suture repair for abdominal wall hernia treatment. However, questions remain regarding the properties of these devices and their influence on surgical outcomes. Morphological properties, including pore size and porosity, play a crucial role in mesh integration and encapsulation. In this study, we introduce a straightforward image analysis procedure for accurately calculating both textile porosity and effective porosity. The latter specifically considers pores that prevent bridging, providing valuable insights into mesh performance.

*Methods:* A photographic setup was established to capture high-quality images of the meshes, accompanied by calibration images necessary for computing the effective porosity. The developed image analysis procedure comprises seven steps focused on improving the binarization process's quality, followed by the computation of textile and effective porosities. To facilitate usability, an app called "poreScanner" was designed using MATLAB app designer, guiding users through the algorithm described herein. The app was used to compute both porosities on 24 meshes sourced from various manufacturers, by averaging seven measurements obtained from as many images. The app's measurement stability was validated computing the coefficient of variation for both textile and effective porosity, for a total of 36 results (24 for the textile porosity and 12 for the effective one). Additionally, different operators independently tested one heavy and one light mesh, confirming the measurement's operator independence.

*Results:* The results on the coefficient of variation indicated values below 5 % in 34 out of 36 cases, regardless of the mesh density. Similarly, the same parameter was computed to assess the independence of the procedure from different operators, yielding a maximum value of 1.84 %. These findings confirm the robustness and user-independence of the measurement procedure.

*Conclusions:* The procedure presented in this study is straightforward to replicate and yields dependable results. Its adoption has the potential to standardize the computation of surgical mesh porosity, enabling consistent determination of this crucial morphological parameter.

## 1. Introduction

Hernia surgery is one of the most performed surgical procedures in the European Union: in 2020 it was performed 148.3 times per 100.000 inhabitants on average for inguinal hernia only, despite the influence of the Covid-19 pandemic, which impacted healthcare activities [1]. Currently, hernia surgery is primarily conducted using surgical mesh to cover the defect, which reduces the time required for the procedure as compared to using sutures to close the gap in the muscle sheet. This technique has been shown to have lower recurrence rates than the latter approach [2]. Furthermore, surgical mesh offers the advantage of expanding the range of operable cases, including those previously deemed inoperable using the suture technique [3].

Despite the clear advantages of utilizing surgical meshes, their implantation can induce a series of bodily reactions that may influence the procedure's outcome. These reactions are contingent upon several characteristics of the device, encompassing mechanical and morphological properties. Subsequent to the implantation of a medical device, it indeed triggers the "Foreign Body Reaction" (FBR), a natural occurrence observed during the final stages of the wound healing process [4]. This

* Corresponding author at: Department of Mechanical and Aerospace Engineering at Politecnico di Torino, Corso Duca degli Abruzzi 24, Torino (TO) 10129, Italy.
*E-mail address:* vincenzo.giacalone@polito.it (V. Giacalone).

https://doi.org/10.1016/j.cmpb.2023.107850
Received 18 July 2023; Received in revised form 5 October 2023; Accepted 6 October 2023
Available online 9 October 2023

process involves the formation of a fibrous capsule, commonly referred to as encapsulation. Although the FBR is a natural response that cannot be prevented, its intensity can negatively impact the performance of the mesh, leading to adverse events like pain and discomfort. This phenomenon arises when fibrous material bridges the gaps between mesh threads, which is influenced by pore dimensions and the quantity of implanted material (namely, the mesh weight) [5]. In this regard, the classification of meshes based on weight allows for the distinction between heavyweight (density $> 90$ g/m$^2$), mediumweight (50 g/m$^2$ $\leq$ density $\leq 90$ g/m$^2$), lightweight (35 g/m$^2$ $\leq$ density $< 50$ g/m$^2$) and ultralightweight (density $< 35$ g/m$^2$) meshes [6]. Several studies have demonstrated a link between the porosity and dimensions of pores of the mesh and the intensity of the FBR, showing that: (1) meshes with greater pore size and porosity (lightweight meshes) can reduce this reaction [7–9]; (2) morphological properties of the mesh exert a more significant influence than the constituent material on the FBR and the formation of adhesions between the mesh and the bowel [10]. However, an excessive reduction of density could lead to an insufficient mechanical strength, which can compromise the stability of the implant [11].

Despite the significance of porosity and pore dimensions as important parameters, some authors have emphasized the lack of a standardized protocol for facilitating comparisons between different device types [12,13]. Several experimental approaches have concentrated on calculating the three-dimensional textile porosity, which is defined as the ratio of the pore volume to the total volume of the mesh. However, these methods have proven to be time-consuming, destructive, and prone to inaccuracies due to the mesh deformation that occurs during testing [13]. To tackle these challenges, alternative studies have employed image analysis techniques for assessing the porosity of surgical meshes. These methods involve calculating a two-dimensional porosity by quantifying the proportion of the mesh's total area occupied by pores: a first approach can be found in Pourdeyhimi et al. [12]. This approach entails converting the image to binary form and determining the textile porosity by calculating the ratio of white pixels (representing pores) to the total number of pixels in the image. A problematic aspect of this approach is that the binarization process relies on selecting a threshold based on the mean of the gray level histogram, without employing additional techniques to enhance the process. Additionally, important details (such as image resolution) are not provided, making it difficult to replicate the procedure.

The *textile porosity* offers insights into the mesh characteristics prior to implantation, disregarding the FBR. To assess post-implantation effects, it is necessary to consider pore dimensions. Pourdeyhimi and colleagues measured pore diameter but, due to the non-circular nature of pores in surgical meshes, this computation may only approximate their actual size. Moreover, at the time of publication, an optimal pore size of approximately 100 μm was acknowledged for achieving favorable outcomes, as the primary emphasis was on attaining robust implant integration [14].

More recently, Mühl et al. [15] proposed a novel image analysis method that accounts for the latest findings on the impact of pore dimensions on the bridging effect, introducing a new measure called *effective porosity*, which considers pores with dimensions greater than 1 mm (found by Klinge et al.[16] to be effective in reducing scar formation *in vivo* on a rat model) as void. Thus, the *effective porosity* is the ratio between the area of the pores that will not be completely bridged by the connective tissue after implantation and the total area of the mesh. To achieve this, they established a setup comprising an industrial camera with a frame grabber card, two stepping motors, and a frame. Up to 100 images of the same sample were captured while the motors moved the mesh. Subsequently, the images were merged prior to porosity computation. However, replicating this setup presents challenges due to the multiple components involved and the non-straightforward assembly process.

In this study, we propose a simplified procedure inspired by the setup presented by Mühl et al., offering a more reproducible approach for calculating both textile and effective porosity from images. Our objective is to establish a new benchmark for comparing surgical meshes. The image processing is streamlined through the utilization of a MATLAB algorithm, implemented in a freely available app named *PoreScanner* [17]. This app facilitates image calibration, binarization, and computation of the relevant parameters. The proposed procedure has been validated on 24 surgical meshes sourced from various manufacturers, accompanied by a usability test of the app to improve the user interface and demonstrate result consistency regardless of the user.

## 2. Materials and methods

### 2.1. Mesh and calibration images acquisition

To accurately determine the textile porosity and effective porosity through image analysis, obtaining high-quality images is a crucial initial step. Therefore, a dedicated photographic setup was created, consisting of a full-frame digital camera (Canon EOS 5D Mark II) equipped with a macro photography autofocus lens (Canon EF 100 mm f/2.8 Macro USM). The camera was securely positioned using a holder, while a bubble level ensured the perpendicular alignment between the camera and the mesh. For optimal contrast, the mesh was positioned on a black cardboard surface, elevated by a support. The mesh was firmly secured using four screws, utilizing the movable cover of the support. Photographs were captured in a windowless room, and uniform exposure conditions for all meshes were achieved by employing a ring light (26 cm in diameter, equipped with 120 dimmable LEDs). The set-up configuration is illustrated in Fig. 1.

In this setup, the distance between the mesh and the camera was set at 17 cm. While reducing this distance could potentially enhance image resolution, extremely short distances may result in the mesh being out of focus. Hence, the chosen distance represents the minimum value that ensured the mesh remained in focus. Additionally, the distance between the cardboard and the mesh (height of the support, h) was fixed at 55 mm. This arrangement preserves the black background in contrast to the translucent mesh, which could appear gray if placed directly on the cardboard surface.

Calibration of the shooting parameters is crucial to obtain suitable images for subsequent post-processing. The shooting parameters requiring calibration include ISO, Av (aperture), and Tv (shutter speed), collectively known as the Exposure Triangle.

For the development of the presented method, meshes were categorized into two groups based on their weight since, in the authors' experience, heavier meshes are typically associated with lower porosity values and vice versa. Circular specimens of meshes with a diameter of 5.5 cm were thus weighted on a digital balance and the mass per unit

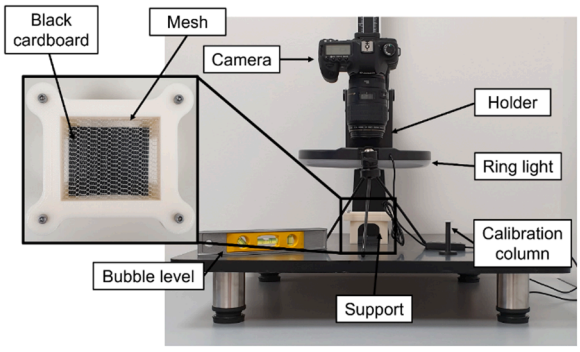


**Fig. 1.** Photographic setup and its function: the holder maintains the camera still; the bubble level ensures the perpendicular alignment between the camera and the mesh; the ring light allows for uniform exposure conditions for the meshes; the calibration column is used to calculate a conversion factor. Top-down view of the mesh support in the zoomed image: the mesh is fixed with four screws, while the black cardboard is used to enhance the contrast.

area in g/m$^2$ was computed. The first group comprised heavyweight meshes, while the second group consisted of mediumweight, lightweight, and ultralightweight meshes. In the subsequent sections of the article, the first group will be referred to as "heavy," and the second group as "light". Due to the varying properties of the heavy and light groups, two distinct sets of shooting parameters were established using a "trial and error" approach (Table 1).

Furthermore, the intensity of the ring light was adjusted according to the density of the meshes. Higher intensity (50 % of the maximum ring light intensity) was used for the heavy group, while lower intensity (20 % of the maximum ring light intensity) was used for the light one. The captured images have a resolution of 3744×5616 pixels (equivalent to 6 μm/pixel).

Calibration images were obtained using the same photographic setup as the mesh images, utilizing a small column with a known diameter and height (Fig. 2b). These calibration images are employed to calculate a conversion factor (*pixel-to-mm*), essential for determining pore dimensions and calculating the effective porosity. To maintain consistency in the focal plane, the height of the column is intentionally set equal to the height of the support (h) (Fig. 2a). It is crucial to exercise caution during the acquisition of both mesh and calibration images, as any modifications to the setup, such as altering the camera orientation or focus, will necessitate repeating the calibration process.

### 2.2. Image processing and porosity calculation

The entire analysis procedure is carried out using MATLAB (version R2021b) and it involves four phases: the calibration, the seven-steps procedure for image binarization, the calculation of textile porosity, and the calculation of effective porosity.

#### 2.2.1. Calibration

The calibration phase enables obtaining the conversion factor (pixel-to-mm) by using a known dimension, which is the diameter of the column (16.059 mm, obtained from an average of 10 measurements taken with a digital caliper). The diameter in mm was compared with the same dimension in pixels, which was calculated using the built-in MATLAB function *imfindcircles* to avoid the influence of manual computation.

#### 2.2.2. Seven-steps procedure for image binarization

The mesh image binarization is obtained through a seven-steps procedure, aimed at enhancing the quality of the binarization process. The first (non-mandatory) step is cropping: cropping allows the definition of a region of interest (ROI) of the same dimension for different acquisition batches, and it is obtained combining the *getpts* and *imcrop* functions to define the position of the upper left corner of the cropped image and its dimensions, respectively. The optimal dimensions were defined as 35 mm x 24 mm to make sure to include more than one repetitive unit for both the heavier and the lighter meshes and to reduce the edge effects for the calculation of the effective porosity (see paragraph 2.2.3). The dimensions are converted to pixels using the conversion factor previously computed.

The cropped RGB mesh image is then converted in grayscale through the built-in MATLAB function *im2gray*, which computes the value of a single pixel based on its R, GandB (Eq. (1)):

$$\text{Grayscale} = 0.2989 * R + 0.5870 * G + 0.1140 * \text{B} \quad (1)$$

The contrast is then enhanced using the function *imadjust* and,

**Table 1**
Shooting parameters for heavy and light groups.

| | Heavy meshes | Light meshes |
|---|---|---|
| ISO | 400 | 250 |
| Av | 14 | 14 |
| Tv | 1 | 2 |

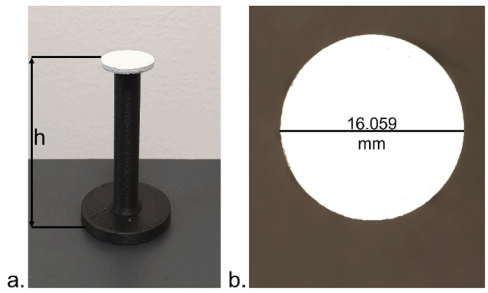


**Fig. 2.** Calibration column (a) and calibration picture (b).

through a thresholding, the binarized image is obtained. After a trial-and-error process, the binarization threshold value was set to 35 for both the heavy and the light groups. The result of this raw binarization is showed in Fig. 3(4) as a yellow mask superimposed on the original cropped image. As visible, few thread areas may be not correctly identified (white arrows in Fig. 3(4)), and this led to a dilatation and erosion process, aimed at improving binarization.

The dilatation process (Fig. 3(5)), indeed, broadens white regions while reducing black ones and has the aim to close small voids inside the threads. The function *imdilate* was used with a circular structuring element having a radius equal to 3 for both the heavy and the light groups. A disadvantage of the dilatation is that certain small pores are reduced in area (red arrows in Fig. 3). For this reason, an erosion is carried out, which expands black regions while restricting the white ones and aims at obtaining a more precise profile of the pores. The function *imerode* was used with a circular structuring element with radius equal to 7 for the heavy groups and to 5 for the light one (see paragraph 2.2.4). The updated binarized image is shown in Fig. 3(6). The first six automatic steps described so far may lead to small residual errors, which are addressed in the seventh and final manual step, aimed at the elimination of residual wrong voids within the threads (green arrows in Fig. 3(7)) by user selection on the image. Here, *getpts* was used to interactively select the wrongly identified pores.

#### 2.2.3. Textile and effective porosities calculation

The textile porosity is calculated as the ratio between the pixels corresponding to pores and the totality of the image pixels [15]. The effective porosity is determined by excluding any pores where the distance between threads is less than 1 mm [16]. The criterion for determining effective porosity based on thread distance is considerably more stringent compared to the one based on pore area alone. This is because a pore may have a large area, even if it is a tight and elongated pore, larger than the area of a circle with a diameter of 1 mm. The pores to be excluded were therefore selected computing through the *regionprops* function the minimum Feret diameter of each pore. The Feret diameter is defined as the length between two parallel lines tangential to a particle's silhouette and the minimum Feret diameter is the smallest of all the possible Feret diameters of the closed area (Fig. 4).

Focusing on the minimum Feret diameter distributions for a light mesh and a heavy mesh (Fig. 5), the absence of pores above the 1 mm threshold in the heavy mesh stands out (Fig. 5a), resulting in an effective porosity equal to zero. On the contrary, light meshes pores appear distributed around the threshold (Fig. 5b).

Effective porosity computation is influenced by the image cropping step. Indeed, pores that fall over the crop area may mistakenly be eliminated because resulting in a minimum Feret diameter below 1 mm, even though their original dimension is above the threshold. The impact of this edge effect on the effective porosity calculation increases with decreasing size of the crop square and increasing pore size. With smaller crops, a greater percentage of pores will be located on the edges relative to the total number of pores in the image, while larger pores will result in a lower number of pores in the image and an increase in the percentage

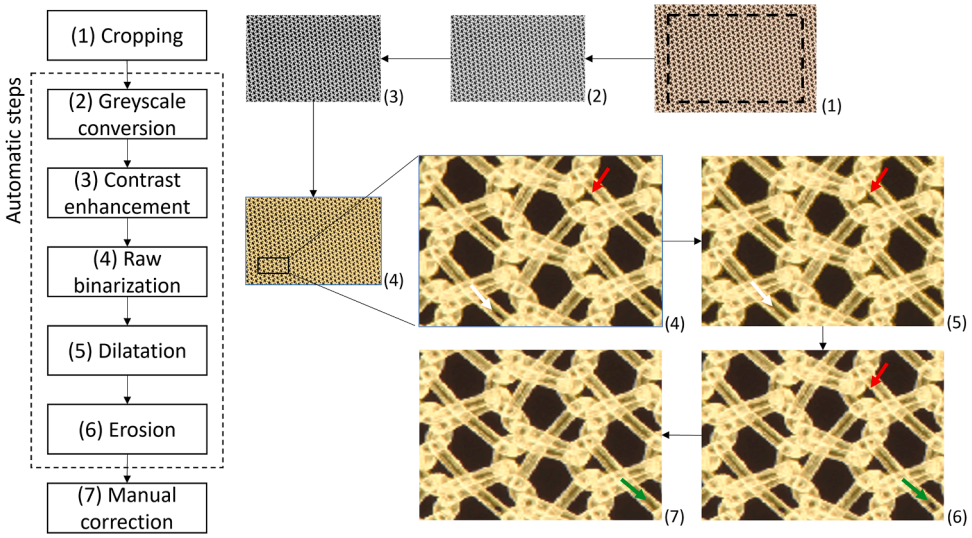


**Fig. 3.** Seven-steps procedure for mesh image binarization, with focus on: the effect of raw binarization on threads detection (white arrows); the effect of dilatation on small pores (red arrows); the manual filling of wrong pores (green arrows).

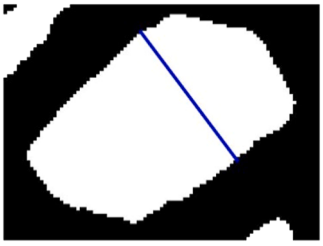

**Fig. 4.** Minimum Feret diameter for a generic pore.

of pores located on the edges. To evaluate this edge effect on the effective porosity calculation, two different crop sizes (10 mm x 10 mm and 24 mm x 24 mm) were compared using the same original light mesh image (Fig. 6). A light mesh has been selected because heavy meshes have pores with minimum Feret diameter smaller than 1 mm, resulting in an effective porosity of zero, regardless of the crop size. For each crop size, five crops were generated from the image, and the effective porosity was automatically calculated based on the minimum Feret diameter criteria. A manual selection of pores having a minimum Feret diameter greater than 1 mm but excluded due to the crop was then performed, to compute a manually corrected effective porosity.

A larger crop results effective in reducing the edge effect (Table 2), leading to a 0.39 % error with a 24 mm x 24 mm square. For subsequent calculations a crop of 35 mm x 24 mm has been chosen to include even more pores in the cropped area and thus reducing further the edge effect. The only exception was that of the slings, in which the height of the rectangle is limited by the dimensions of the device.

### 2.2.4. *Erosion radii tuning*

The tuning of the erosion parameter was performed on a heavy mesh (HM0) image and a light mesh (LM0) image, on which the binarization procedure was performed varying the erosion radius. For each erosion radius tested, the diameters of the threads were manually computed using the built-in MATLAB function *imtool* and compared with the thread nominal diameter declared by the manufacturer.

Given the image resolution of about 6 μm per pixel, a one-pixel error would induce a 6 % or a 10 % error on the heavy group (180 μm thread diameter) and the light group (120 μm thread diameter) respectively. The aim of the tuning process was to obtain a mean error equal to zero on the computation of the diameter of the threads. To achieve this result,

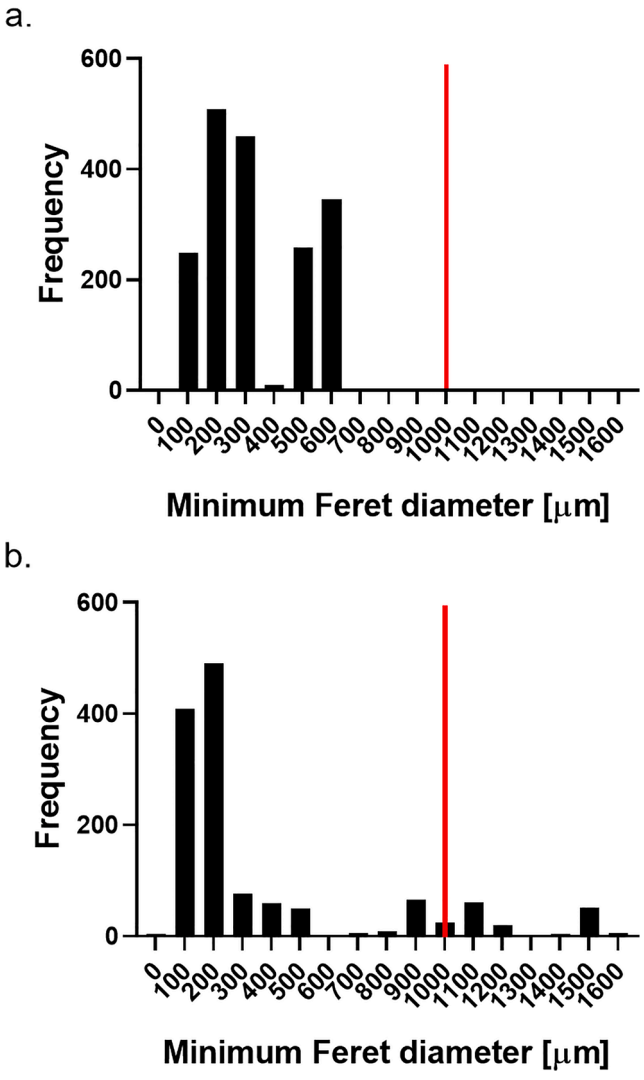


**Fig. 5.** Pores distribution for a heavyweight mesh (a) and for a lightweight mesh (b); pores with a minimum Feret diameter above the 1000 μm threshold will be counted for the computation of the effective porosity.

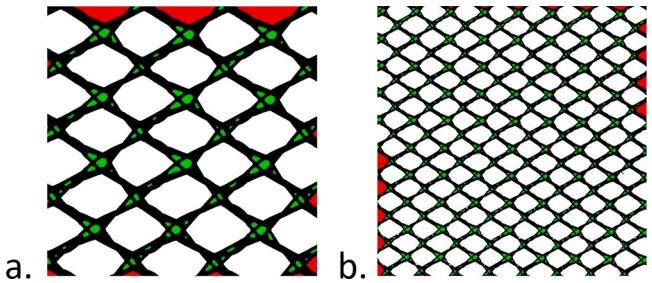


**Fig. 6.** Automatic and manual pores selection according to the minimum Feret diameter criteria in (a) the 10 mm x 10 mm and (b) the 24 mm x 24 mm crop sizes. The green areas indicate the pores correctly eliminated with the automatic control, while the red areas indicate the edge pores wrongly eliminated with the automatic control and included by the manual control.

**Table 2**
Edge effect on the effective porosity induced by different crop sizes. Effective porosities are computed as average of five measures.

| Crop size | 10 mm x 10 mm | 24 mm x 24 mm |
|---|---|---|
| **Effective Porosity (Automatic computation)** | 65.19 % ± 0.64 % | 66.38 % ± 0.07 % |
| **Effective Porosity (Manual correction)** | 66.35 % ± 0.67 % | 66.77 % ± 0.08 % |
| **Error** | 1.16 % | 0.39 % |

the erosion parameter was changed accordingly, recognizing that structuring elements with larger radii produce a more powerful erosion effect.

Starting from a radius equal to 6 px, the diameters of ten threads were therefore measured and the percentage error E was calculated according to Eq. (2):

$$E = \frac{D_c - D_n}{D_n} * 100 \quad (2)$$

Where:

$D_c$ is the computed diameter;

$D_n$ is the nominal diameter (180 μm and 120 μm for the heavy and light groups, respectively).

A positive value of E would trigger the selection of a bigger radius and vice versa.

#### 2.2.5. *Verification of the seven-steps procedure*

The validation rationale was based on the hypothesis that a correct computation of the porosity is a consequence of a correct identification of threads and voids, and therefore of a correct segmentation (i.e. binarization) of the image. Since, to the best of the authors' knowledge, there are no gold standard experimental methods for the computation of the two-dimensional porosity, and no reference specimen with a known two-dimensional porosity is available to test the algorithm developed, the ability to maintain the diameter of the threads equal to their nominal value during the binarization phase was analyzed. For this purpose, it was assumed that the forming process does not alter the nominal diameter.

The seven-steps procedure was thus tested on five additional meshes using the erosion values found in the tuning phase according to mesh density. The percentage error E was calculated according to Eq. (2).

#### 2.2.6. *poreScanner app usability and repeatability testing*

An app (*poreScanner* [17]) was created using the MATLAB app designer which guides users through the presented algorithm to facilitate the seven-step procedure. Its outputs are the mask image, an image showing the original image with the mask superimposed in transparent yellow, and an Excel file. The app is freely available (https://doi.org/10.5281/zenodo.8161015) and does not require MATLAB. It only requires MATLAB runtime which will be automatically installed with the app. Specific system requirements for MATLAB runtime can be found in the MathWorks website [18]. Since the output of the app is an Excel file, it is necessary to have an Office license.

To ensure the usability of the app, a test was conducted to identify and rectify any critical issues. Five operators were provided with a user manual and used the app. Their feedback was then utilized to modify any part of the user interface or manual that was unclear to users.

After optimization, the app was used with 24 meshes from various manufacturers, each with a different weight. The textile and effective porosities of each mesh were computed by averaging seven measurements obtained from as many images. To assess the stability of the algorithm, the coefficient of variation (CV) was calculated for each of the 24 meshes by dividing the standard deviation of the seven measurements by their mean. This was done for each textile porosity measurement and for each effective porosity value different from zero, for a total of 36 values.

In addition, one new heavy mesh and one new light mesh were tested by five different operators to confirm the independence of the measurements from the operator, with a specific focus on the last step of manual control. To ensure consistency, the operators used the same crop size to prevent any edge effects from influencing the calculation of effective porosity. To assess the intersubject variability, the coefficient of variation (CV) was calculated for each of the 2 meshes by dividing the standard deviation of the five measurements (one for each operator) by their mean.

## 3. Results

### 3.1. *Erosion radii tuning and seven-steps procedure verification*

The erosion radius was adjusted by performing the binarization procedure on the HM0 and LM0 images, while varying the erosion radius until achieving the lowest average percentage error. The rationale behind this choice is related to the fact that a null average error indicates a compensation for overestimation and underestimation of threads diameter, and thus of the overall area occupied by the threads. The optimized radii for the two mesh groups were found to be 7 px for the heavy group and 5 px for the light group, as shown in Fig. 7a. The average percentage errors computed in the tuning phase result, indeed, lower than 0.81 %.

The tuned erosion radii performed effectively when applied to a broader range of mesh weights, spanning from light to heavy (Fig. 7b), also confirming the choice to discriminate the binarization parameters on the basis of the mesh weights (see Supplementary material). The average errors remained consistently lower than 5 %. With the 5 px radius the average error is indeed 1.5 %.

### 3.2. *poreScanner app usability and repeatability testing*

To establish a reliable and reproducible method, two key aspects required verification. The first aspect involved assessing the stability of measurements obtained from different images of the same mesh. As stated in paragraph 2.2.6, this was achieved by calculating the coefficient of variation (CV) for each of the 24 meshes, considering both the textile and effective porosity. In total, 36 CVs were computed (24 for the textile porosity and 12 for the effective one) from the porosity results represented in Fig. 8.

The obtained CVs are below 5 % in 34 out of 36 measures (Fig. 9), assessing the stability of the measurements, throughout the wide range of porosity results analyzed. The higher CV values for the heavy group can be explained by the fact that heavier meshes have lower values of porosity: while the values of standard deviation are comparable to that of the light group, the mean values are lower, resulting in greater CVs. In fact, the mesh with the higher value of CV (6.44 %) is also the mesh with the lowest porosity value (mean value of 15.02 %). In the light group,

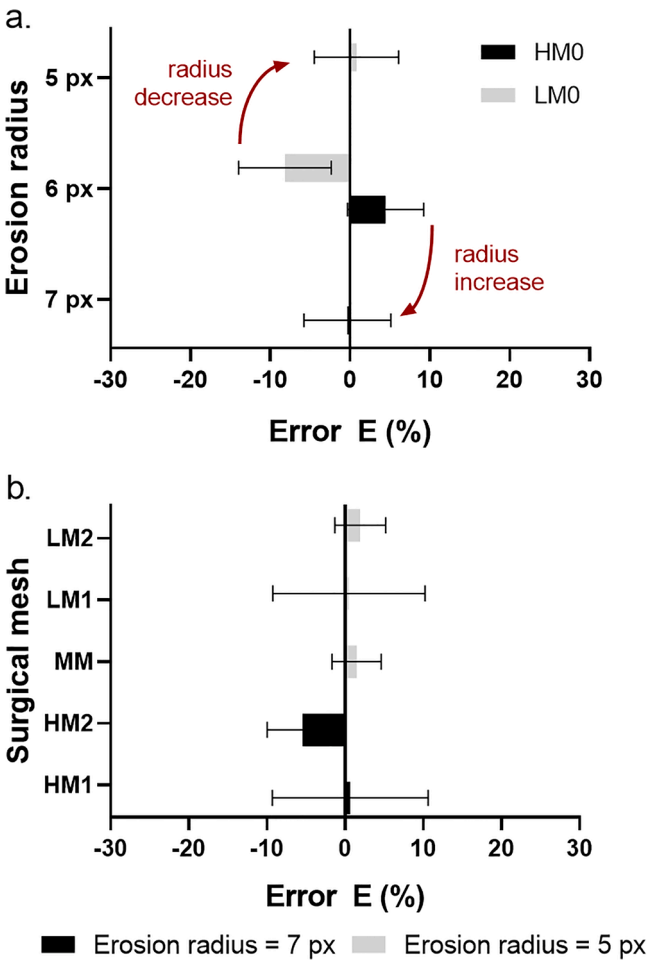


**Fig. 7.** Tuning of the erosion radii for the heavy and light meshes according to the mean percentage error (a) and testing of the tuned radii on 5 new meshes characterized by different densities (b).

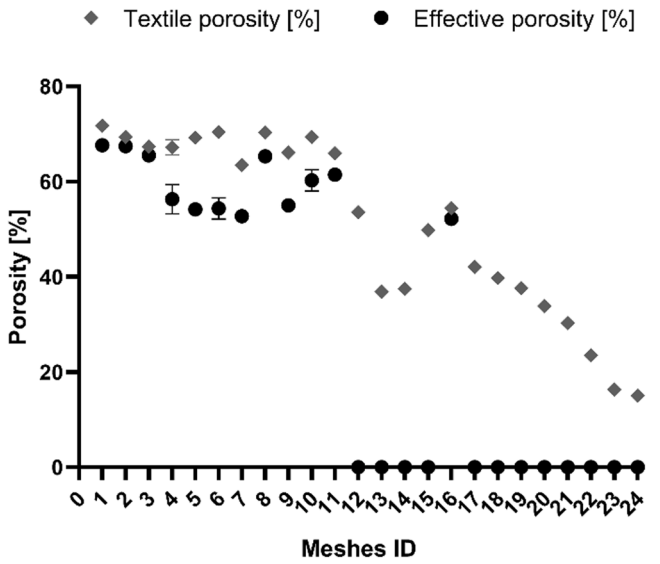


**Fig. 8.** Mean porosity values computed for each device. Error bars are not shown when the standard deviation is less than 1.6. See Table S1 of the supplementary material for the raw data.

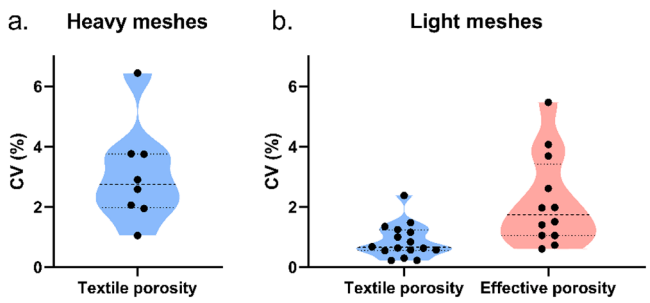


**Fig. 9.** Violin plots of the coefficients of variation computed for the heavy (a) and light (b) meshes. For heavy meshes, it should be noted that the effective porosity is equal to zero.

the higher CV values for the effective porosity result from variations in the proportion of pores with different shapes and dimensions across the seven images of the same mesh. Considering this, the recommendation is to capture images with an equal proportion of different pore shapes to further reduce the already low variability observed in these cases. This is especially true in the more porous meshes.

The second aspect verified was the repeatability of the procedure when different operators used the app. Changing the number of residual wrong voids eliminated during the manual correction could significantly alter the proportion of black and white pixels, consequently affecting the porosity values in a non-negligible manner. Therefore, the coefficient of variation (CV) was computed again, this time focusing on the difference in textile and effective porosities obtained using two pictures, as described in Paragraph 2.2.6. The results are presented in Table 3, which confirms the minimal variation between the results obtained by different operators. As the effective porosity for the heavy mesh is zero, this result is not included in the table.

## 4. Discussion

The lack of international standards and shared protocols among researchers presents a major challenge in studying surgical meshes [19, 20]. Therefore, it is crucial to establish new methodologies that are easy to replicate, enabling research groups to effectively compare their results. This work aims to address this need by simplifying the experimental set-up presented by Mühl [15] and providing a free-to-use app for porosity computation.

The simplification was achieved by eliminating the merging process of the pictures, demonstrating that a picture size greater than approximately 20 mm per side is sufficient to make the edge effect negligible while maintaining a resolution of the images comparable, if not better, than the one reported in Mühl's work (10 μm). Here, a maximum resolution of about 6.55 μm is achieved. This also eliminates the need for two stepping motors since there is no requirement to move the probe during the test. Additionally, the image quality is suitable for the post-processing phase even when using a cheap impinging light source instead of a LED screen. Furthermore, the rest of the set-up, including the holder and the calibration column, can be easily and economically 3D printed (https://doi.org/10.5281/zenodo.8161015). The only initial financial investment required was for the camera lens.

The computation of the effective porosity was also simplified, substituting a sequence of dilations and erosions with the computation of the Feret diameter, using a MATLAB tool.

**Table 3**
Coefficient of variation for repeatability test.

| | Heavy mesh | Light mesh |
|---|---|---|
| Textile porosity | 1.75 % | 0.52 % |
| Effective porosity | – | 0.84 % |

The choice of dividing meshes into two groups based on their weight is justified by the results showed in Fig. S1a and b which demonstrate a better correlation between weight and textile porosity than between diameter and textile porosity. This fact can be explained since while it is true that changing the diameter of the threads could result in different porosity values, it is also true that lower porosity values can be obtained with the same diameter simply changing the stich density of the threads, as found in the literature [21]. Fig. S1c shows that the correlation with weight is reduced when looking at the effective porosity ($R^2 = 0.52$); this happens because, over a certain weight, effective porosity values become equal to zero. This highlights how textile porosity alone is not sufficient to have a complete insight into the mesh behavior, hence the need for a tool that computes both porosities.

The main limit of a two-dimensional technique is principally the impossibility of linking the 2D porosity with the real three-dimensional one. However, the leading aim of the study was the standardization of a method for the computation of mesh porosities and image analysis technique was chosen due to its simpler reproducibility compared with experimental tests. It must be also highlighted that the method performs effectively only when the starting pictures are taken in a specific manner, even though the actions needed to accomplish the correct result are finely explained in the paper.

Another limitation is due to the lack of a reference specimen with a known two-dimensional porosity that could have provided a real validation for the entire procedure. Nevertheless, the results presented in paragraph 3.1 reassure on the reliability of the output provided by the algorithm: the tuning phase confirm the precision of the measures, showing a mean error on the measured diameters lower than 5 %, while the coefficients of variation (Fig. 9) confirm the repeatability of the procedure. The seventh step for the removal of residual errors could cause some variability between different users, but this step is mostly not necessary if the procedure presented here for the acquisition of the images is followed; even when this step is used, the difference between operators is low, proving the stability of the first six steps (see Table 3).

Finally, the implementation of the seven-step procedure in the *poreScanner* app can encourage the acquisition of the same method by other research groups, and this is only possible choosing an image analysis technique. Moreover, the collaboration with other researchers could provide further ideas for the improvement of the algorithm. As stated at the beginning of the paragraph, the uniformity of method between researchers and companies has a great significance when speaking about properties of devices that have a direct impact on the patient's safety, and this uniformity is still lacking in the literature, as evidenced by the widely varied results obtained, even when using the same method, such as image analysis (Table S2, Supplementary material).

The importance of morphological properties of surgical meshes, in fact, has been recognized since the second half of the nineties: Arnaud et al. [22] compared mesh materials with non-porous materials used for the repair of hernia, showing that the formers perform better, while Amid [23] classified mesh materials into four classes based on the dimensions of their pores. However, these early studies focused on the dimensions of pores useful for avoiding complications like seromas, infections and adhesions, while granting a strong incorporation of the implant: the heavy meshes were the most used in this period[6]. There was no consideration of other complications like pain and foreign body sensation, both due to the morphological properties of the mesh materials other than the mechanical ones [24]. More recently, Klinge et al. [16] proved a reduced level of inflammation and fibrosis when using low weight meshes compared to high weight meshes in a study on rats. Additionally, there is a proven link between the intensity of the inflammation and complications like paraesthesia, pain, shrinkage and adhesions [25]. For this reason, in the last years the focus of the research moved to lighter meshes, which have typically greater porosity than the heavy ones. As highlighted by Mühl, the real link between host reaction and morphological properties of the implant is the effective porosity, which considers the shape of the pores and not only the proportion of voids and threads in the mesh. This parameter suggests that meshes with different textile porosity, will cause the same reaction once implanted if they have the same effective porosity [26], even though, as Conze et al. point out [7], the ingrowth of fibrocollagenous material is not to be considered always a negative event: for example, in the laparoscopic hernia repair, a sufficient ingrowth is needed to withstand the intra-abdominal pressure. Based on this evidence, Klinge et al. proposed a new classification method for meshes, based on their effective porosity [26].

In the future, the algorithm presented here will be integrated with the capability to compute other morphological parameters based on the binarized images. Examples include the distribution of pore area within the device and pore orientation. Subsequent versions of the app may incorporate these additional parameters, providing new insights into mesh properties.

## 5. Conclusion

The aim of this article is to provide an easily reproducible way of computing textile and effective porosity of surgical meshes through image analysis. The verification phase proved the reliability of the procedure, showing that the algorithm has a mean error on the diameter of the threads equal to zero, irrespectively of the mesh density. Moreover, the results of the repeatability test highlight the independence of the procedure from the user. The focus on the porosity was chosen by the increasing number of studies linking this parameter to the outcome of the surgical procedure and in particular with some adverse events. Even if more knowledge in the field is needed to better understand the link between porosity and host response, in authors opinion the use of the same method would allow different researchers and companies to link the outcome of different implants with an important design parameter, giving surgeons a more reliable way to choose the better implant for a specific application.

## Funding

The first author's scholarship is funded by the European Union – NextGenerationEU.

## Declaration of Competing Interest

The authors declare that they have no known competing financial interests or personal relationships that could have appeared to influence the work reported in this paper.

## Supplementary materials

Supplementary material associated with this article can be found, in the online version, at doi:10.1016/j.cmpb.2023.107850.

## References

[1] ES, Explained Surgical operations and procedures performed in hospitals, Eurostat (2020) 1–11. http://ec.europa.eu/eurostat/statistics-explained/index.php/Surgical_operations_and_procedures_statistics#In-patient_procedures:_cataract_surgery Explained.

[2] A.J. Aldridge, D. Nehra, Mesh compared with non-mesh methods of open groin hernia repair: systematic review of randomized controlled trials and laparoscopic compared with open methods of groin hernia repair: systematic review of randomized controlled trials, Br. J. Surg. 88 (3) (2001) 471, https://doi.org/10.1046/j.1365-2168.2001.01762-7.x.

[3] G.M. Larson, H.W. Harrower, Plastic mesh repair of incisional hernias, Am. J. Surg. 135 (4) (1978) 559–563, https://doi.org/10.1016/0002-9610(78)90037-5.

[4] J.M. Anderson, A. Rodriguez, D.T. Chang, Foreign body reaction to biomaterials, Semin. Immunol. 20 (2) (2008) 86–100, https://doi.org/10.1016/j.smim.2007.11.004.

[5] J.M. Bellón, M. Rodríguez, N. García-Honduvilla, V. Gómez-Gil, G. Pascual, J. Buján, Comparing the behavior of different polypropylene meshes (heavy and lightweight) in an experimental model of ventral hernia repair, J. Biomed. Mater.

Res. B Appl. Biomater. 89 (2) (2009) 448–455, https://doi.org/10.1002/jbm.b.31234.
[6] S. Kalaba, E. Gerhard, J.S. Winder, E.M. Pauli, R.S. Haluck, J Yang, Design strategies and applications of biomaterials and devices for Hernia repair, Bioact. Mater. 1 (1) (2016) 2–17, https://doi.org/10.1016/j.bioactmat.2016.05.002.
[7] J. Conze, R. Rosch, U. Klinge, et al., Polypropylene in the intra-abdominal position: influence of pore size and surface area, Hernia 8 (4) (2004) 365–372, https://doi.org/10.1007/s10029-004-0268-8.
[8] K. Junge, U. Klinge, R. Rosch, B. Klosterhalfen, V. Schumpelick, Functional and morphologic properties of a modified mesh for inguinal hernia repair, World J. Surg. 26 (12) (2002) 1472–1480, https://doi.org/10.1007/s00268-002-6444-z.
[9] L. Zogbi, E.N. Trindade, M.R.M. Trindade, Comparative study of shrinkage, inflammatory response and fibroplasia in heavyweight and lightweight meshes, Hernia 17 (6) (2013) 765–772, https://doi.org/10.1007/s10029-013-1046-2.
[10] D.A. Raptis, B. Vichova, J. Breza, J. Skipworth, S. Barker, A comparison of woven versus nonwoven polypropylene (PP) and expanded versus condensed polytetrafluoroethylene (PTFE) on their intraperitoneal incorporation and adhesion formation, J. Surg. Res. 169 (1) (2011) 1–6, https://doi.org/10.1016/j.jss.2009.12.014.
[11] C.R. Deeken, M.S. Abdo, M.M. Frisella, B.D. Matthews, Physicomechanical evaluation of polypropylene, polyester, and polytetrafluoroethylene meshes for inguinal hernia repair, J. Am. Coll. Surg. 212 (1) (2011) 68–79, https://doi.org/10.1016/j.jamcollsurg.2010.09.012.
[12] B. Pourdeyhimi, Porosity of surgical mesh fabrics: new technology, J. Biomed. Mater. Res. 23 (13 S) (1989) 145–152, https://doi.org/10.1002/jbm.820231313.
[13] F. A, H.E. Deeb, H.A. Taleb, R A, Determination of pore size, porosity and pore size distribution of woven structures by image analysis techniques, J. Text Sci. Eng. 07 (05) (2017), https://doi.org/10.4172/2165-8064.1000314.
[14] J.D. Bobyn, G.J. Wilson, D.C. MacGregor, R.M. Pilliar, G.C. Weatherly, Effect of pore size on the peel strength of attachment of fibrous tissue to porous-surfaced implants, J. Biomed. Mater. Res. 16 (5) (1982) 571–584, https://doi.org/10.1002/jbm.820160505.
[15] T. Mühl, M. Binnebösel, U. Klinge, T. Goedderz, New objective measurement to characterize the porosity of textile implants, J. Biomed. Mater. Res. B Appl. Biomater. 84 (1) (2008) 176–183, https://doi.org/10.1002/jbm.b.30859.
[16] U. Klinge, B. Klosterhalfen, V. Birkenhauer, K. Junge, J. Conze, V. Schumpelick, Impact of polymer pore size on the interface scar formation in a rat model, J. Surg. Res. 103 (2) (2002) 208–214, https://doi.org/10.1006/jsre.2002.6358.
[17] Giacalone V., Civilini V., Audenino A., Terzini M. poreScanner (1.0). Published online 2023. https://zenodo.org/record/8161015.
[18] MathWorks. System requirements and supported compilers. Accessed April 12, 2023. https://it.mathworks.com/support/requirements/previous-releases.html.
[19] S. Todros, P.G. Pavan, P. Pachera, A.N. Natali, Synthetic surgical meshes used in abdominal wall surgery: part II—Biomechanical aspects, J. Biomed. Mater. Res. B Appl. Biomater. 105 (4) (2017) 892–903, https://doi.org/10.1002/jbm.b.33584.
[20] V. Civilini, V. Giacalone, A.L. Audenino, M. Terzini, A reliable and replicable test protocol for the mechanical evaluation of synthetic meshes, J. Mech. Behav. Biomed. Mater. 144 (2023), 105987, https://doi.org/10.1016/j.jmbbm.2023.105987.
[21] L. Miao, F. Wang, L. Wang, T. Zou, G. Brochu, R. Guidoin, Physical characteristics of medical textile prostheses designed for hernia repair: a comprehensive analysis of select commercial devices, Materials 8 (12) (2015) 8148–8168, https://doi.org/10.3390/ma8125453.
[22] J.P. Arnaud, R. Eloy, M. Adloff, J.F. Grenier, Critical evaluation of prosthetic materials in repair of abdominal wall hernias. New criteria of tolerance and resistance, Am. J. Surg. 133 (3) (1977) 338–345, https://doi.org/10.1016/0002-9610(77)90542-6.
[23] P.K. Amid, Classification of biomaterials and their related complications in abdominal wall hernia surgery, Hernia 1 (2) (1997) 70, https://doi.org/10.1007/bf02427664.
[24] M.M. Uzzaman, K. Ratnasingham, N. Ashraf, Meta-analysis of randomized controlled trials comparing lightweight and heavyweight mesh for Lichtenstein inguinal hernia repair, Hernia 16 (5) (2012) 505–518, https://doi.org/10.1007/s10029-012-0901-x.
[25] K. Baylón, P. Rodríguez-Camarillo, A. Elías-Zúñiga, J.A. Díaz-Elizondo, R. Gilkerson, K. Lozano, Past, present and future of surgical meshes: a review, Membranes 7 (3) (2017) 1–23, https://doi.org/10.3390/membranes7030047.
[26] U. Klinge, B. Klosterhalfen, Modified classiffication of surgical meshes for hernia repair based on the analyses of 1,000 explanted meshes, Hernia 16 (3) (2012) 251–258, https://doi.org/10.1007/s10029-012-0913-6.